Pure and Applied Geophysics

Ground Motion Zoning of Santiago de Cuba: An Approach by SH Waves Modelling

Leonardo Alvarez[1,2], Julio García[1], Franco Vaccari[3,4],
Giuliano F. Panza[2,4], Bertha González[1], Carmen Reyes[1],
Bárbara Fernández[1], Ramón Pico[5], José A. Zapata[1],
and Enrique Arango[1]

Abstract — The expected ground motion in Santiago de Cuba basin from earthquakes which occurred in the Oriente fault zone is studied. Synthetic *SH*-waves seismograms have been calculated along four profiles in the basin by the hybrid approach (modal summation for the path source-profile and finite differences for the profile) for a maximum frequency of 1 Hz. The response spectra ratio (RSR) has been determined in 49 sites, distributed along all considered profiles with a spacing of 900 m. The corresponding RSR versus frequency curves have been classified using a logical-combinatorial algorithm. The results of the classification, in combination with the uppermost geological setting (geotechnical information and geological geometry of the subsoil) are used for the seismic zoning of the city. Three different main zones are identified, and a small sector characterized by major resonance effects, due to the particular structural conditions. Each zone is characterized in terms of its expected ground motion parameters for the most probable strong earthquake ($M_S = 7$), and for the maximum possible ($M_S = 8$).

Key words: Synthetic seismograms, surface waves, zoning, Santiago de Cuba.

Introduction

In a previous paper, the realistic modelling of *P-SV* and *SH* waves for a frequency up to 1 Hz was done for two profiles in Santiago de Cuba city (ALVAREZ *et al.*, 2001a). Those results show the influence of the basin structure on the ground motion, and indicate the limits and possibilities of using the modelling of waves propagation for microzoning purposes. Within the framework of UNESCO/IUGS/ IGCP Project 414 "Realistic modelling of seismic input for megacities and large urban areas", it has been decided to refine those results by using more detailed information about the shallow geology (geotechnical information, and geological

---

[1] Centro Nacional de Investigaciones Sismológicas, Cuba (CENAIS).
[2] The Abdus Salam International Centre for Theoretical Physics, Italia (ICTP).
[3] Istituto Nazionale di Geofisica e Vulcanologia - Osservatorio Vesuviano, Naples, Italy (INGV-OV).
[4] Dipartimento di Scienze della Terra, Università di Trieste, Italia (DST).
[5] Instituto de Cibernética, Matemática y Física, Cuba (ICIMAF).

geometry of the subsoil) and regional deep structure, and to extend them to all the present and perspective areas of the city. Santiago de Cuba is the second most populated city of Cuba. Located close to the boundary between the Caribbean and North American plates, it is exposed to a relatively high level of seismic hazard (ALVAREZ *et al.*, 1999; RODRÍGUEZ *et al.*, 1997). Earthquakes felt in the city with I = VIII degrees on the MSK scale, have a recurrence period of about 80 years and there exists a high probability of occurrence of a $M_S = 7$ earthquake in the near future (RUBIO, 1985) close to the city, in the Oriente transform fault system. This hypothetical earthquake is used as ''scenario'' for calculating synthetic seismograms along four profiles in the city by the hybrid technique (FÄH, 1992; FÄH *et al.*, 1993, FÄH and PANZA, 1994) based on modal summation and finite differences. The procedure computes wavetrains generated by a seismic source buried in a regional crust-upper mantle structure (bedrock), and uses this motion as input to the local structure. The signals in the bedrock anelastic structure are generated by the modal summation approach (PANZA, 1985; PANZA and SUHADOLC, 1987; FLORSCH *et al.*, 1991; PANZA *et al.*, 2000); the waveforms along the local, laterally varying anelastic structure are then computed using a finite-difference scheme (VIRIEUX, 1984, 1986; LEVANDER, 1988) applied to the local structure. The results of the modelling are used to make the seismic zoning of the local structure, using as zoning criteria the ''response spectra ratio'' (RSR), i.e., the spectral amplification defined by:

$$RSR = [Sa(2D)/Sa(1D)]$$

where Sa(2D) is the response spectrum (at 5% of damping) for the signals calculated in the laterally varying structure, and Sa(1D) is the one calculated for the signals in the bedrock regional reference structure.

Geological Setting of the Santiago de Cuba Basin

Santiago de Cuba is characterized, from the geological point of view, by rocks, and stiff and unconsolidated sediments of different age, origin and lithological composition. The study region of the present work covers an area of approximately 250 km^2. Recently, the analysis of new borehole data, as well as detailed field surveys, have supplied a more detailed geological map of Santiago de Cuba basin (MEDINA *et al.*, 1999). Following those authors, three kinds of geological formations are present in the basin:

- *Formations of the Paleogene Volcanic Arc*. El Cobre Group is made up of several formations with a great complexity from the lithological point of view. It mainly consists of conglomerates and sandstones with tuffaceous composition, gravelites, tuffs, tuffites and limestones with lava flows of intermediate composition. They outcrop at the west and at the north of the study region and are presumed to be

the bedrock foundation of the basin. This zone is not included in our study, because the development of the city is not oriented in that direction, due to its topographic characteristics.

- *Neogene rocks.* La Cruz formation comprises three members: Quintero, Tejar and Santiago. It is composed of polimitic conglomerates, calcarenites, argilites, calcareous sandstones, marls and reef sandstones, as well as of calcareous silts and sandy argilites. All members are represented in Santiago de Cuba city and its surroundings.

- *Quaternary formations.* They are of several kinds. The first one mainly comprises gravelly alluvium (gravels, sands and clays with calcareous composition). We can find these soils mostly filling river basins, such as the San Juan River basin in the eastern part of the city. The second kind can be identified bounding the Santiago de Cuba and Cabañas bays, and is composed of sandy clays and peat, as well as man-made ground and bay mud. Additionally present are the formations Camaroncito, Jaimanitas and Rio Maya, characterized by different kinds of limestone.

Three faults cross the basin (ARANGO, 1996; PÉREZ and GARCÍA 1997). They are denominated El Cristo (present in the northwestern part of the study region), Bahía (along the eastern board of Santiago de Cuba Bay) and Sardinero (in the southeast corner of the study region).

A compilation of the structural parameters, geotechnical information, and geological geometry of the subsoil in Santiago de Cuba was constructed in the form of a database containing more than 600 boreholes' data. The quality of these data is variable consisting, in the main, of visual description and classification of strata. The depth of penetration of boreholes varies: the majority reaches less than 25 m, there are 83 between 25 and 50 m, 31 between 50 and 120 m and only 3 reach approximately 200 m of depth.

Using these data, the generalized geological zoning has been performed, compiling a set of maps representing the setting at different depths (5 m intervals close to the surface, 10–20 m intervals from 80 to 200 m). In the compilation of these maps, the real, very detailed lithological composition has been considered. The analysis of these maps, together with the consideration of the intervals of variation of the physical-mechanical properties of the rocks present in the geological maps, permitted us to simplify and generalize the map of MEDINA *et al.* (1999). The result of this generalization is shown in Figure 1. As can be seen from the figure, only six kinds of soils are present, corresponding to sands and sandstones of Quaternary formations, clays, sands and magmatic intrusions from Neogene formations, calcareous rocks and limestones from Neogene and Quaternary formations, as well as volcano-clastic rocks, tuffs, tuffites and agglomerates of El Cobre formation of the Paleogene Volcanic Arc. Additionally, significant lenses of gravelly alluvium (gravels, sands and clays with calcareous composition) are present at depth in different parts of the basin.
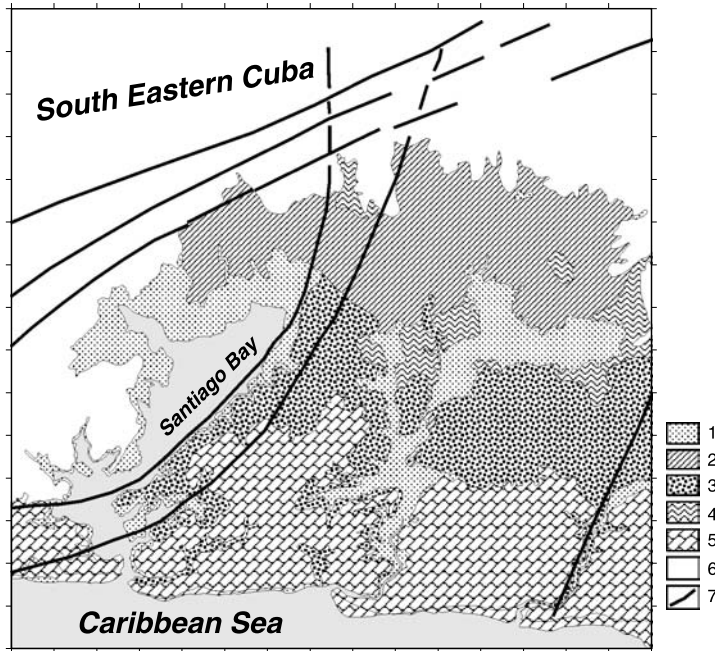
Figure 1

Simplified geological scheme of Santiago de Cuba basin (modified from MEDINA *et al.*, 1999), 1—sand and sandstones (Quaternary formations), 2—clays (Neogene), 3—marls (Neogene), 4—magmatic intrusions, 5—calcareous rocks and limestones (Neogene and Quaternary formations), 6 — rocks from El Cobre formation (Paleogene Volcanic Arc), 7—faults; the ticks on the frame of the figure are 1 km apart, the left-low corner has coordinates 19.954°N and 75.897°W.

Regional Structural Model

The crust structure in the region is very complicated, as can be seen in ALVAREZ *et al.* (2001b) and we will use only a simplified regional model, consisting of a slight modification of the anelastic parameters of structure *L* of the cited paper (Figure 2). This was constructed, for a depth less than 30 km, using the contribution of ARRIAZA (1998), who reinterpreted the results of BOBENKO *et al.* (1980), while for depths ranging from 30 to 150 km the results of the *P*-wave tomography study of VAN DER HILST (1990) and of the gravimetric study of ORIHUELA and CUEVAS (1993) have been considered. For depths greater than 150 km, the standard oceanic model of HARKRIDER (1970) is used.

The upper frequency limit for the numerical simulation has been fixed at 1 Hz. Although approximate, it is accepted that such results are pertinent for buildings of ten storys and more, lifelines, etc. This kind of building exists in Santiago de Cuba city since approximately 15 years ago, when a program of construction of typical 12-, 15- and 18-story buildings began. A recent study of the microseisms spectral content,
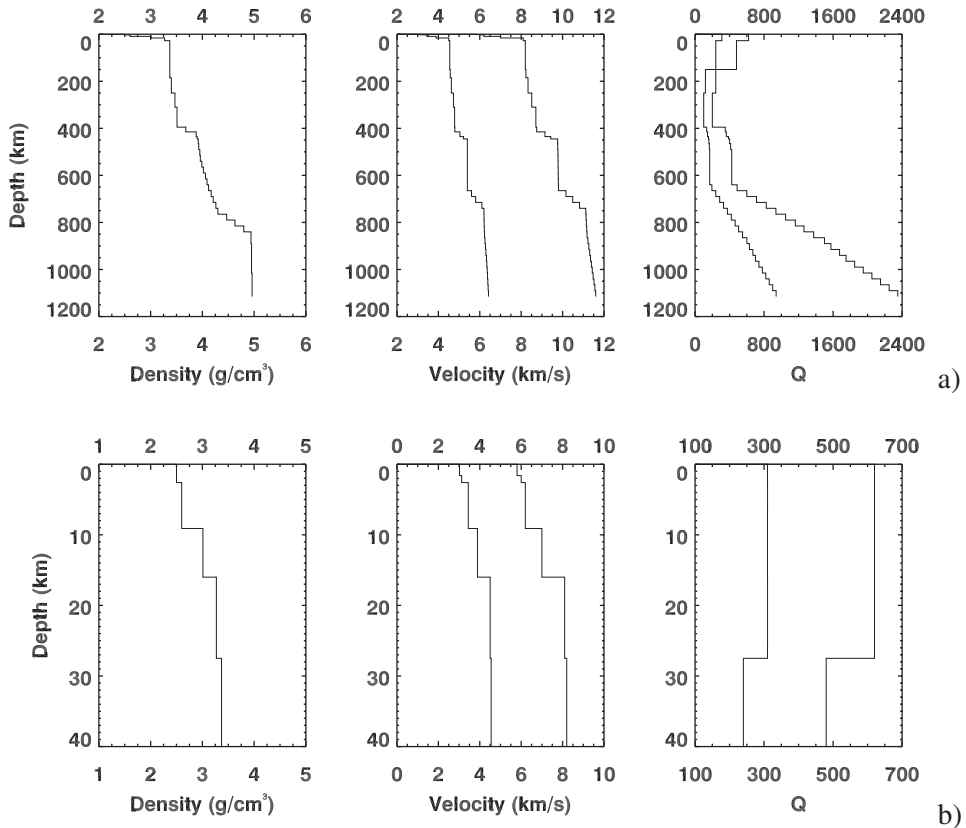
Figure 2
a) Regional structural model; b) detail of the first 40 km.

based on *in situ* measurements at the base and at the last floor of the buildings indicates that free oscillation periods of 18-story buildings range from 0.8–1.2 seconds (GONZÁLEZ, 1998; SEO *et al.*, 1998), and it is known that these periods tend to increase with the ageing of the building. Consequently, our results will be useful for future city planning and for mitigation of the seismic risk to existing buildings.

Two Dimensional Structural Profiles in the Basin

For studying the influence of the sedimentary basin structure on the seismic input, four profiles were selected across the basin. They follow the conditions that all the zones present in the simplified geological scheme of Figure 1 are sampled (only the small bodies of magmatic intrusions were not included) and that the traces pass

close to the places where the deeper boreholes of our database are located. The corresponding cross sections have been prepared using, for depth < 50 m, mainly boreholes' data from a band 0.25 km wide at both sides of each profile trace. More distant boreholes have been used for larger depths, reaching 210 m. The cross sections show smooth transitions through the different zones and sharp ones when crossing the fault present in the study area. The data pertaining to the mechanical properties (*P*- and *S*-wave velocities and quality factors) of the strata (see Table 1) were taken from the literature (PAVLOV, 1984; ISHIHARA, 1993; BERGE-THIERRY *et al.*, 1999), as no direct measurements were available. Nevertheless, the selected values are in correspondence with other measurements made on similar soils elsewhere in Cuba. The density is supported by laboratory measurements data, present in our database. The grid used in the finite-difference calculations was selected with dimension, at the surface, $\Delta x = \Delta z = 0.015$ km, in agreement with the details given in the sections.

The sources are placed on the Oriente transform fault system at 30 km of depth and at a distance of 25 km from the coast, in the main seismogenetic zone that affects the region, where the expected strong earthquakes are likely to be located. In Figure 3 the locations of sources and the profiles's traces are shown.

Results

a) Synthetic Seismograms

Synthetic seismograms for *SH* waves have been calculated along the selected profiles in the city by the hybrid approach (FÄH, 1992, FÄH *et al.*, 1993). The sites are placed on the surface with a fixed spacing of 900 m. For each site we calculate displacement, velocity and acceleration seismograms for a point source with seismic moment $Mo = 1.0 \times 10^{13}$ N-m, focal depth $h = 30$ km, and focal mechanism: dip = 21°, azimuth = 302° and rake = 21°. This mechanism corresponds to the

Table 1

Physical properties of the different layers present in the selected profiles

| No.	Brief Description	V_P (Km/s)	V_S (Km/s)	ρ (g/cm^3)	Q_P	Q_S
1	Sands	1.2	0.35	1.8	100	50
2	Clays	0.8	0.3	1.6	100	50
3	Marls	1.3	0.6	2.0	150	50
4	Calcareous soils	0.9	0.5	1.8	150	50
5	Calcareous rocks	2.5	1.4	2.3	200	100
6	Igneous rocks	2.4	0.8	2.1	350	150
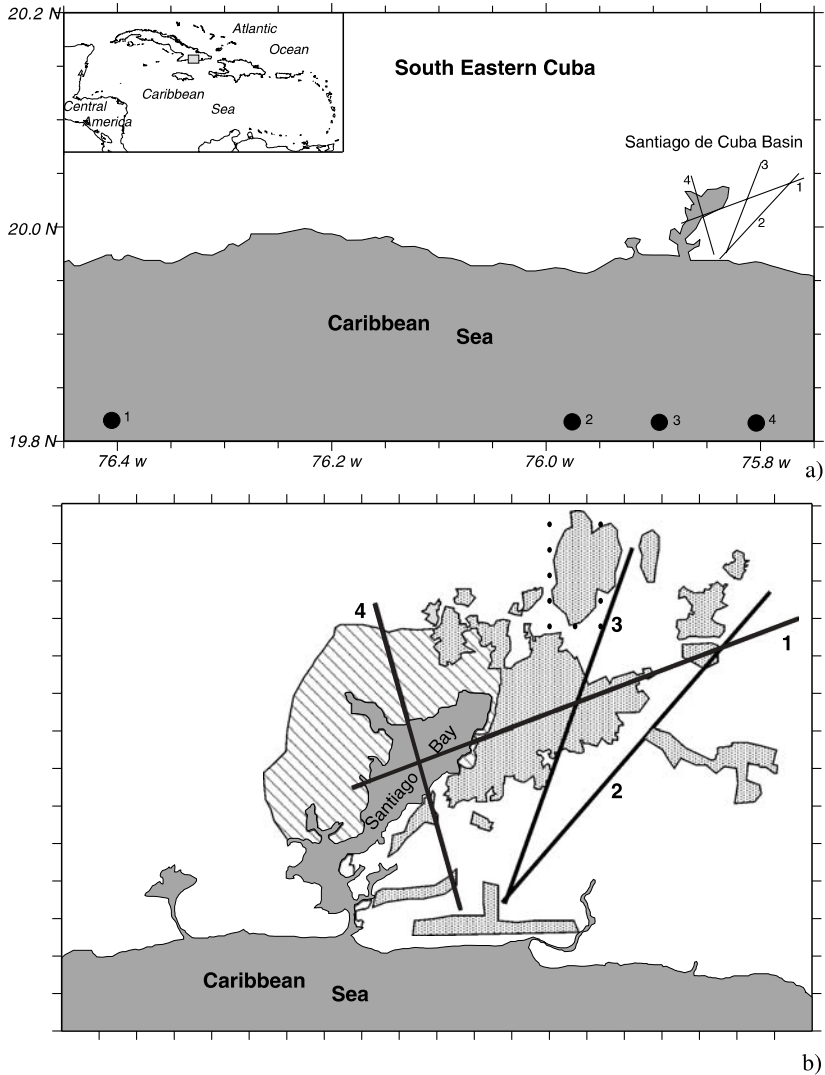
Figure 3
a) Position of the sources and profiles; b) detail of profile traces in the basin and city plan (dotted areas correspond to human settlements, hatched areas correspond to industrial areas). The ticks on the frame of the figure are 1 km apart, the left-low corner has coordinates 19.945°N and 75.945°W.

Harvard University determination of one local earthquake that can be considered representative of the seismic sources in this sector of the Oriente fault zone. These seismograms then have been scaled in the frequency domain (PANZA *et al.*, 1996) for possible earthquakes of different magnitudes by using the scaling law of GUSEV (1983), as reported by AKI (1987).

The "response spectra ratio" (RSR), as has been expressed before, is used as the basis of the zoning of the city. The plots of RSR, as functions of frequency and position along the profiles, are shown together with the corresponding cross sections in Figure 4. The RSR is larger and more variable for frequencies greater than 0.4 Hz. At the end of profile 2 a clear resonance effect, characterized by very high values that correspond in the time domain to long wave trains is present. Additionally, the occurrence of two kinds of patterns is clear. Those corresponding to profiles 2 and 3
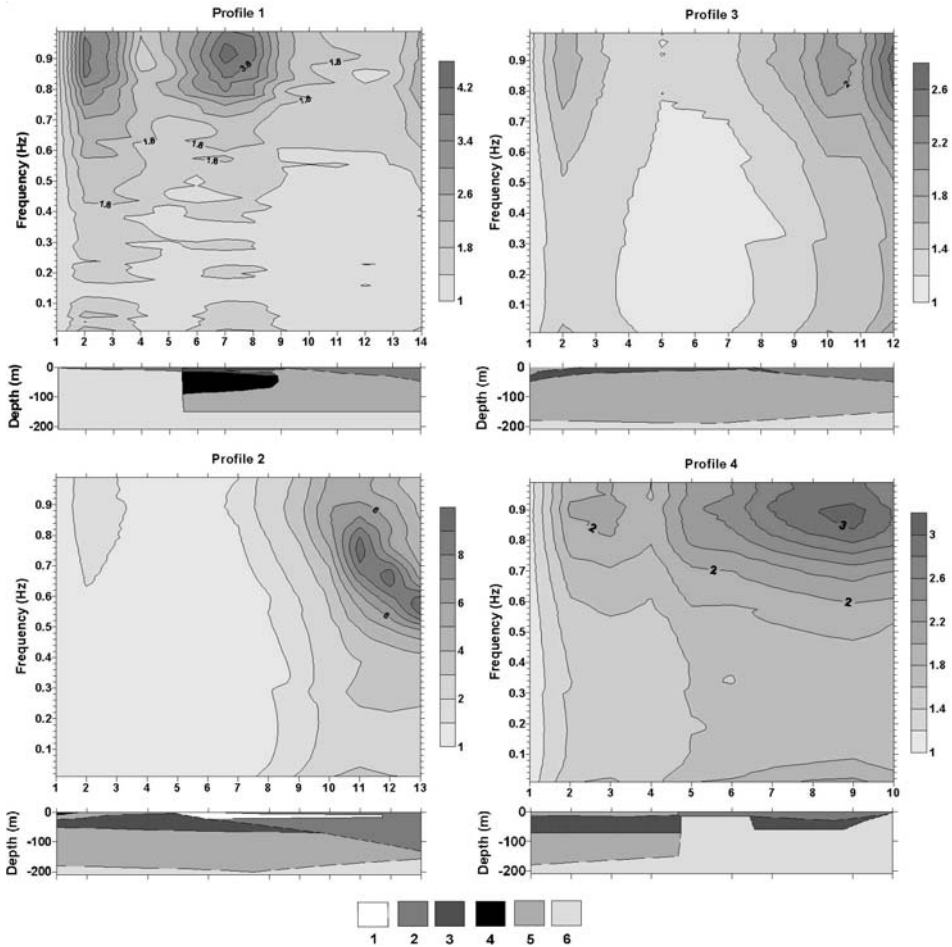

Figure 4

Relative response spectra (RSR) of SH waves as a function of frequency along each profile. The models of each profile are plotted below each panel. The numbers along the *x* axes correspond to the ordinal site position. The epicentral distances of the first site in profiles 1, 2, 3 and 4 are 103.9 km, 43.5 km, 34.5 km and 33.6 km, respectively. Along each profile, the distance between two adjacent sites is 900 m. The numbering in the legend corresponds to the different layers, whose parameters are given in Table 1.

are relatively smooth, in accordance with the smooth variation of the layering, while the ones corresponding to profiles 1 and 4 present rapid variations that are well correlated with the sharp lateral boundaries in the layers, due to the presence of a fault.

b) RSR Curves Classification

The RSR vs. frequency curves have been analyzed in order to make the zoning of the basin. The RSR data for each site are sampled at 0.05 Hz from 0.39 to 0.99 Hz for a total of 13 points at each site. The obtained 49 curves are shown in Figure 5. These data are processed, for the classification in compact sets, with a non-supervised logical-combinatorial algorithm included in *PROGNOSIS system* (RUIZ et al., 1992). To perform this analysis the curves are numbered continuously from the first (profile 1) to the last (profile 4), and in each profile from the beginning to the end. The main features of the algorithm are:

- Let the curve number "j" be the object "O_j", and the value of the RSR at frequency number "i" be the variable "x_i". Then, the value of RSR at the frequency number "i" in the curve number "j" will be "$x_i(O_j)$".
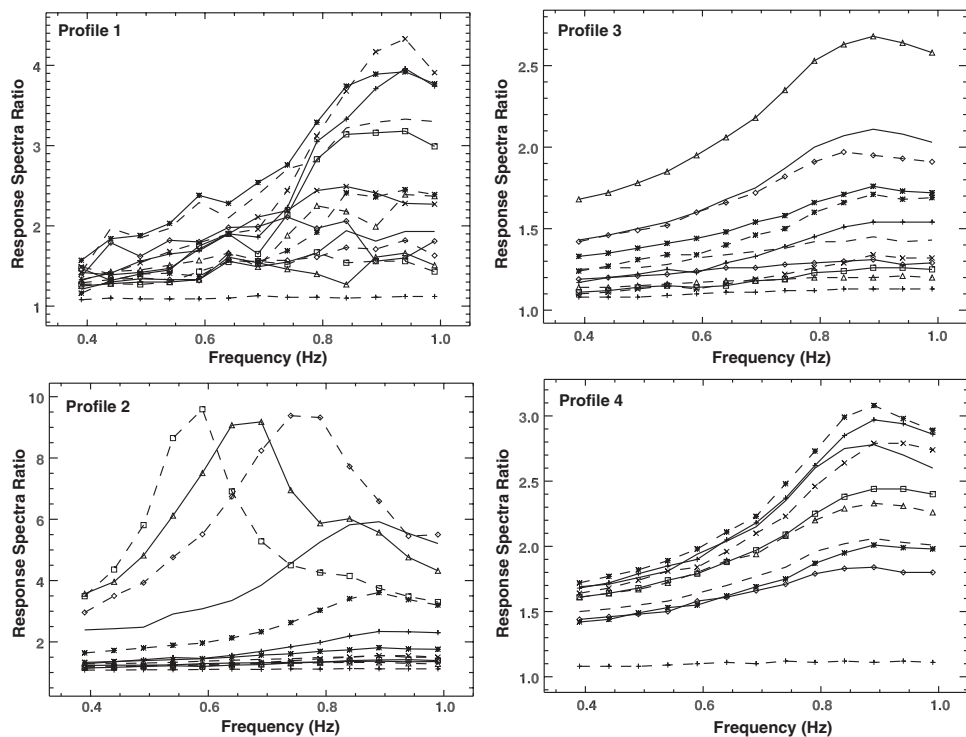

Figure 5
Response spectra curves for all profiles from 0.39 to 0.99 Hz, sampled at 0.05 Hz.

- Let $max(x_i)$ and $min(x_i)$ be the extremes of the variable x_i over all the objects. The similarity between objects is calculated by the formula

$$S(O_l, O_k) = \frac{1}{n} \sum_{i=1}^{n} \frac{|x_i(O_l) - x_i(O_k)|}{max(x_i) - min(x_i)} \ .$$

- Two objects O_i and O_j are β_o-*similar*, if and only if $S(O_i,O_j) \geq \beta_o$, where β_o, the level of the classification, is between 0 and 1. An object belongs to a compact set if the most similar to it is into this set too, or if it is the most similar to other objects belonging to the set.
- The compact sets are graphically represented in a dendrogram, where the different β_o levels in which they are grouped can be seen. Selecting interactively over this scheme the level β_o, a particular partition in β_o-compact sets can be determined (PICO, 1999).
- The procedure starts determining the main β_o-compact sets; then, some of the sets can be subdivided using additional criteria, and the average curve for each final set is calculated.

Initially, for a level of similarity $\beta_o = 0.25$, nine sets have been obtained. The first one, which comprised many curves with the smaller RSR values present in the data set that form a wide sector in RSR vs. frequency graph, was subdivided in four subgroups attending to the range of variation, in average, of RSR. As a result twelve groups have been identified and their average curves are shown in Figures 6a,b. In the following they will be referred as "typical" curves of the groups.

In this set, 5 limit groups can be isolated. The curves 3, 6, 7 and 8 correspond to the last four sites in profile 2, where the surface waves resonance effect was identified, while curve 10 corresponds to the first sites in each profile, where no RSR increments can be expected. In Figure 7 the results of classification are compared with the geological scheme of the basin. For the seismic zoning, a sort of correspondence between surface geology and RSR level was sought. For mapping our results, a generalization of the 12 typical RSR curves was done. It consists in a grouping of close curves into a common one, considering also the geological characteristics along the profiles. As a result, three such groups were identified: high—(2,5,9), intermediate—(4,12), low—(1,10,11). Consequently, the zoning of the basin was made in terms of these three groups. The boundaries between zones follow, whenever possible, the boundaries between the different elements of the geological map (slightly smoothed). For the zones not crossed by the profiles we took into account the results obtained in similar (by structure in depth) zones crossed by them. The zoning scheme is shown in Figure 8, where the small subzone, corresponding to the sites where the resonance effect has been identified, is delimited by a thick dashed line. The average RSR curves for each zone are shown in Figure 9.
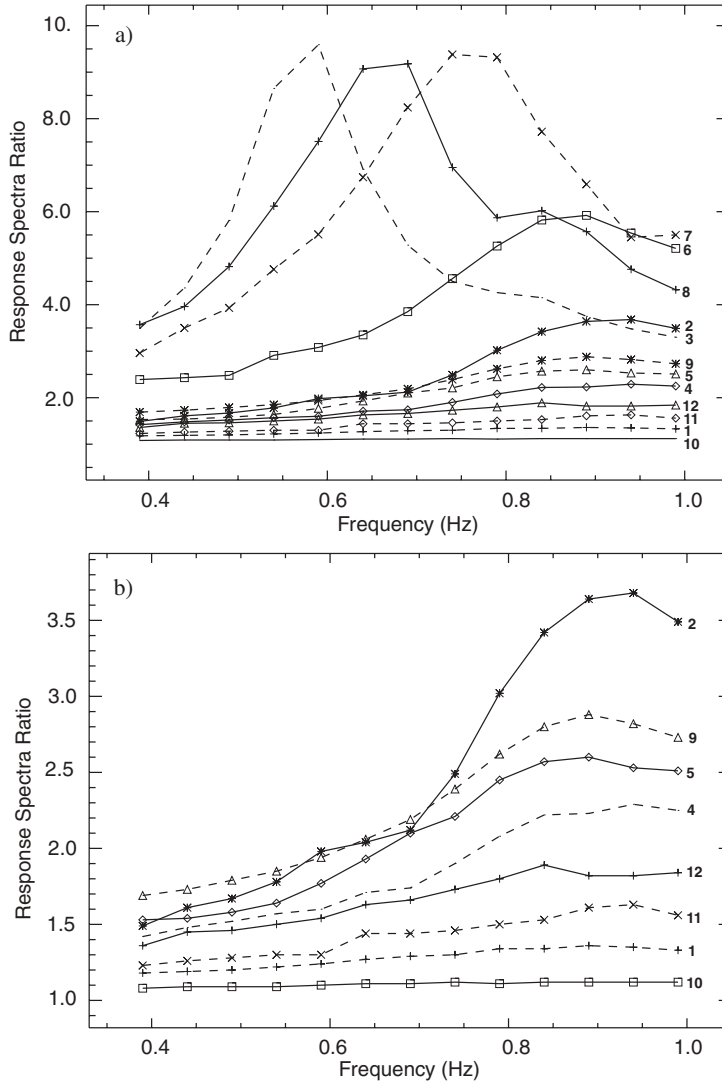
Figure 6
Typical RSR curves versus frequency obtained as a result of the classification procedure. a) All groups;
b) detail after removing the four curves that present anomalous higher values.

c) Expected Ground Motions

For obtaining information about the expected ground motions in the Santiago de Cuba basin, the obtained synthetic signals have been scaled to $M_S = 7$, the most probable strong earthquake, and to $M_S = 8$, the maximum possible earthquake, as estimated from seismotectonic considerations (COTILLA and
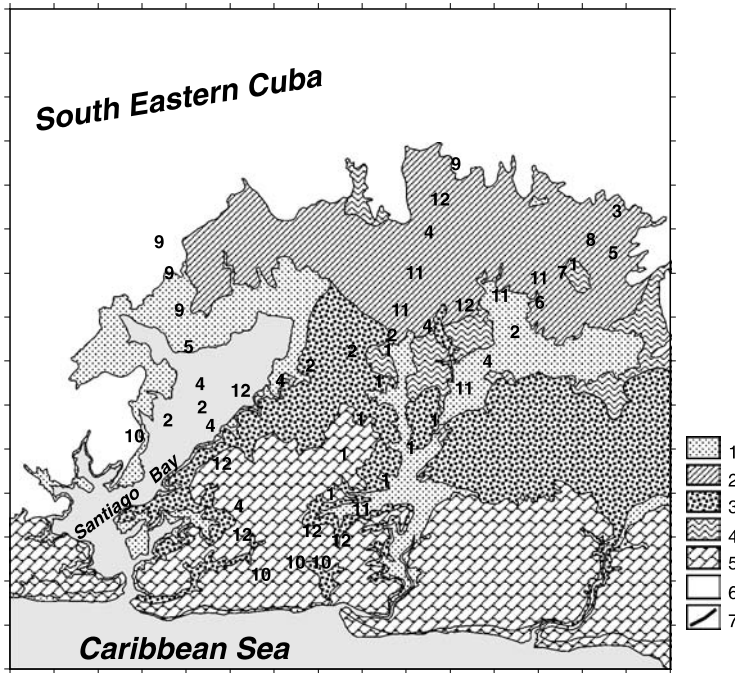
Figure 7
Representation of the results of the classification of all curves over the geological map. The numbers correspond to the typical curves shown in Figure 6, while the legend is equivalent to the one of Figure 1. The ticks on the frame of the figure are 1 km apart, the left-low corner has coordinates 19.954°N and 75.897°W.

ALVAREZ, 1991). From these scaled signals the maximum ground motion displacement (d_{max}), velocity (v_{max}) and acceleration (a_{max}) have been determined. As the frequency content of our signals is out of the range in which the maximum peak values of acceleration are commonly observed, the values of the design ground acceleration (DGA) are obtained by scaling acceleration seismograms with the design response spectra for the soils S1, S2 and S3 of the Cuban building code (NORMA CUBANA, 1999). A rough estimation of the real peak ground acceleration can be obtained from the maximum spectral value MSV, through MSV = 2.5 * DGA. A discussion of this procedure can be found in PANZA *et al.* (1996) and ALVAREZ *et al.* (1999). In Tables 2 and 3 the results for $M_S = 7$ and $M_S = 8$ earthquakes are reported, respectively. Finally, recalling that the Effective Peak Acceleration (EPA) is defined as the average spectral acceleration in the period interval from 0.1 s to 0.5 s divided by 2.5 (APPLIED TECHNOLOGY COUNCIL, 1978), we see that EPA is equivalent to the DGA, calculated using design response spectra.
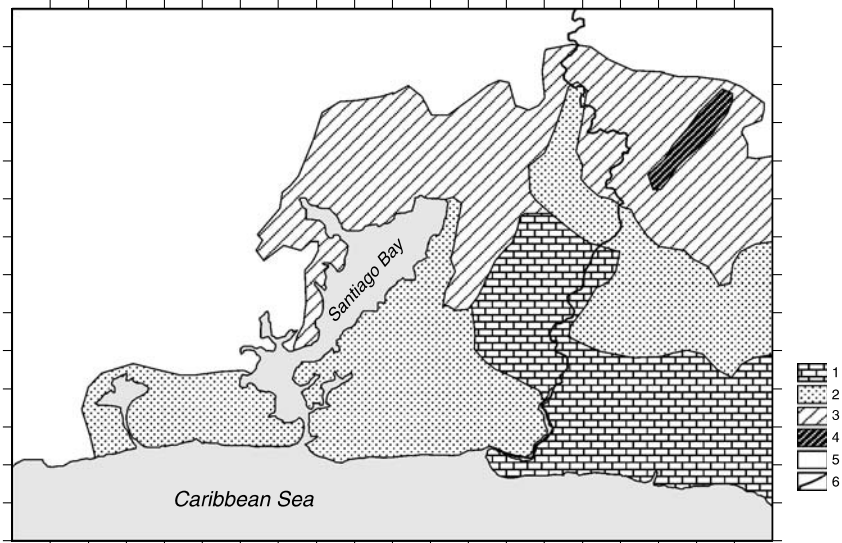
Figure 8

Zoning of Santiago de Cuba basin: 1—low RSR level, 2—intermediate RSR level, 3—high RSR level, 4—subzone, of the previous one, where resonance effect was identified, 5—zone of El Cobre formation, not included in our analysis, 6—San Juan River. The ticks on the frame of the figure are 1 km apart, the left-low corner has coordinates 19.945°N and 75.945°W.
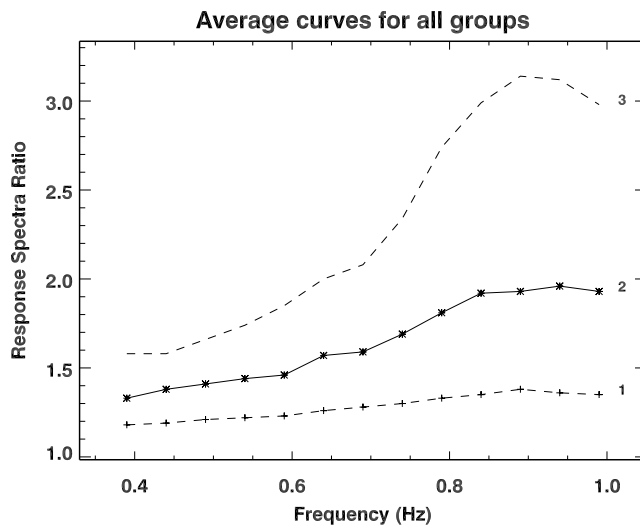
Figure 9

Average RSR curves versus frequency for each zone of the zoning scheme: 1—low RSR level, 2—intermediate RSR level, 3—high RSR level.

Table 2

Ground motion parameters for an earthquake of $M_S = 7$ in the sites located along all the profiles

| No.	d_{max} (cm)	v_{max} (cm/s)	a_{max} (cm/s^2)	DGA$_{S1}$ (cm/s^2)	DGA$_{S2}$ (cm/s^2)	DGA$_{S3}$ (cm/s^2)
Profile 1, $\Delta = 103.9$ km to the beginning of profile					
1	0.23	0.09	0.22	0.74	0.43	0.36
2	0.24	0.13	0.41	1.65	1.12	0.97
3	0.24	0.12	0.39	1.36	0.92	0.80
4	0.24	0.10	0.30	0.99	0.66	0.55
5	0.24	0.11	0.25	0.82	0.55	0.48
6	0.24	0.11	0.28	1.18	0.80	0.70
7	0.24	0.11	0.34	1.46	0.99	0.86
8	0.24	0.10	0.34	1.23	0.83	0.72
9	0.24	0.09	0.28	0.77	0.53	0.46
10	0.23	0.09	0.25	0.76	0.45	0.36
11	0.23	0.09	0.24	0.76	0.45	0.36
12	0.23	0.09	0.22	0.74	0.46	0.39
13	0.23	0.09	0.21	0.74	0.49	0.42
14	0.24	0.10	0.27	0.96	0.64	0.54
Profile 2, $\Delta = 43.5$ km to the beginning of profile					
15	2.48	3.26	9.89	30.14	19.93	16.86
16	2.63	3.89	12.91	41.41	27.71	23.59
17	2.55	3.60	11.65	36.59	24.30	20.61
18	2.48	3.40	10.63	32.90	21.85	18.48
19	2.43	3.32	10.06	31.31	20.66	17.44
20	2.37	3.27	9.64	29.48	19.58	16.56
21	2.32	3.26	9.56	29.26	19.43	16.51
22	2.37	3.60	11.55	36.75	24.79	21.28
23	2.49	4.00	14.48	51.52	34.75	29.83
24	2.74	4.37	18.96	82.81	55.85	47.94
25	2.92	5.06	22.55	149.45	99.24	83.93
26	2.98	5.14	18.93	163.39	107.82	90.49
27	2.96	4.71	16.61	165.08	107.54	89.13
Profile 3, $\Delta = 34.5$ km to the beginning of profile					
28	3.12	3.76	11.94	36.29	24.10	20.38
29	3.31	4.54	15.78	50.88	34.28	29.43
30	3.21	4.23	14.48	44.54	29.81	25.38
31	3.14	4.14	13.73	41.67	27.67	23.55
32	3.07	4.07	12.88	39.27	26.08	22.06
33	3.01	4.12	12.76	38.97	25.97	22.11
34	2.96	4.15	12.71	39.46	26.41	22.48
35	2.97	4.32	13.87	44.58	29.83	25.52
36	2.98	4.47	14.78	47.74	31.95	27.35
37	3.08	4.91	17.47	57.49	38.47	32.83
38	3.02	4.79	16.66	54.92	36.75	31.29
39	3.18	5.48	20.30	70.65	47.28	40.25
Profile 4, $\Delta = 33.6$ km to the beginning of profile					
40	1.87	2.46	7.55	22.77	15.12	12.79
41	2.03	3.16	11.01	36.06	24.32	20.87
42	2.04	3.21	11.43	37.25	25.12	21.56

Table 2

(contd.)

No.	d_{max} (cm)	v_{max} (cm/s)	a_{max} (cm/s^2)	DGA$_{S1}$ (cm/s^2)	DGA$_{S2}$ (cm/s^2)	DGA$_{S3}$ (cm/s^2)
43	1.99	3.10	10.68	34.81	23.30	19.96
44	2.04	3.45	12.31	42.50	28.66	24.60
45	2.02	3.47	12.51	43.47	29.32	25.16
46	2.01	3.60	13.32	47.12	31.78	27.28
47	1.98	3.68	13.82	49.87	33.64	28.87
48	1.96	3.70	13.91	51.18	34.52	29.63
49	1.89	3.49	12.88	46.97	31.68	27.19

Discussion

The RSR patterns show the influence of the different geological features. There is a ''regular'' behavior, characterized by very small RSR values, at small frequencies, followed by a smooth monotonous RSR increment from about 0.4 Hz, until 0.9 Hz, where the relative maximum is reached, and a small decrease until 1 Hz. There are two exceptions to this relatively simple pattern. The first is at the end of profile 2, where the RSR pattern shows the appearance of very large amplitudes in the range 0.6–0.8 Hz, in the form of a narrow peak, followed by a sharp decrease towards 1 Hz. In this part there is a thick clay layer, however before reaching it the waves travel through a structure in which a relatively big lens of sand of the small San Juan River basin is embedded into the clays. It results in a cumulative increase of waves amplitude and duration, which remain after the sand lens is passed. This effect is similar to what has been obtained by ALVAREZ et al. (2001), where the largest RSR values for SH waves, along the San Juan River, were obtained at the sites where the thickness of Quaternary sediments was bigger. The second exception is represented by the oscillating RSR patterns in the entire analyzed frequency range for the profiles 1 and 4, due to the presence of Bahía fault.

Our zoning results are a scheme, not a map, because the density of RSR calculations is not sufficient to construct a map. Figure 8 has been obtained extending our local results to the whole study area. Surface geology alone cannot explain the different RSR patterns found and it is necessary to consider the data of the deeper structure. For example, the limestones in the south of the study region are classified in two different levels: to the west of San Juan River in the intermediate level, while to the east in the low level. This difference is due to the structure at depth; limestones in the west lie over marls, while in the east this layer of marls does not appear.

Table 3

Ground motion parameters for an earthquake of $M_S = 8$ in the sites located along all the profiles

No.	d_{max} (cm)	v_{max} (cm/s)	a_{max} (cm/s^2)	DGA$_{S1}$ (cm/s^2)	DGA$_{S2}$ (cm/s^2)	DGA$_{S3}$ (cm/s^2)
Profile 1, $\Delta = 103.9$ km to the beginning of profile							
1	1.62	0.55	0.94	3.20	1.88	1.58
2	1.62	0.71	1.86	7.56	5.14	4.45
3	1.62	0.66	1.79	6.24	4.24	3.67
4	1.60	0.59	1.29	4.48	2.96	2.48
5	1.58	0.61	1.15	3.69	2.51	2.17
6	1.58	0.62	1.28	5.41	3.68	3.19
7	1.58	0.60	1.51	6.63	4.51	3.91
8	1.58	0.57	1.55	5.62	3.82	3.31
9	1.57	0.51	1.29	3.55	2.42	2.09
10	1.57	0.50	1.13	3.14	1.96	1.62
11	1.56	0.50	1.06	3.19	1.97	1.61
12	1.56	0.50	0.99	3.12	2.05	1.73
13	1.56	0.48	0.96	3.33	2.21	1.87
14	1.57	0.49	1.20	4.31	2.86	2.42
Profile 2, $\Delta = 43.5$ km to the beginning of profile							
15	15.92	14.84	44.33	135.40	89.91	76.14
16	16.50	17.64	58.11	188.10	125.88	107.17
17	16.08	16.28	52.36	165.11	109.93	93.59
18	15.67	15.39	47.52	148.42	98.55	83.36
19	15.39	15.00	44.77	140.42	93.24	78.86
20	15.05	14.88	42.91	133.23	88.47	74.99
21	14.80	14.83	42.97	131.95	88.04	74.96
22	14.97	16.29	52.27	167.51	112.98	96.97
23	15.48	18.04	65.33	237.10	159.92	137.26
24	16.55	19.87	85.05	381.56	257.35	220.89
25	17.25	22.34	1.60	673.84	447.48	380.98
26	17.59	21.59	85.68	720.94	475.74	399.28
27	17.19	21.31	76.39	726.95	473.54	392.50
Profile 3, $\Delta = 34.5$ km to the beginning of profile							
28	16.49	16.92	53.16	164.03	108.92	92.58
29	17.26	20.39	70.54	232.10	156.54	134.37
30	16.78	19.04	65.10	202.42	135.46	115.33
31	16.40	18.66	61.83	188.02	125.57	106.91
32	16.00	18.38	57.89	177.08	117.59	100.01
33	15.68	18.61	57.27	176.34	118.01	100.47
34	15.37	18.72	56.81	179.56	120.17	102.31
35	15.33	19.45	61.94	203.08	135.90	116.61
36	15.32	20.09	66.17	217.45	145.58	124.95
37	15.71	22.11	78.71	262.27	175.51	150.25
38	15.38	21.57	74.95	250.37	167.55	142.65
39	16.00	24.71	91.45	322.09	215.55	183.51
Profile 4, $\Delta = 33.6$ km to the beginning of profile							
40	9.84	11.09	33.72	102.82	68.27	58.06
41	10.49	14.26	49.85	164.17	110.72	95.04
42	10.48	14.54	51.72	170.12	114.40	98.20

Table 3

(contd.)

No.	d_{max} (cm)	v_{max} (cm/s)	a_{max} (cm/s^2)	DGA$_{S1}$ (cm/s^2)	DGA$_{S2}$ (cm/s^2)	DGA$_{S3}$ (cm/s^2)
43	10.17	14.02	47.76	158.69	106.23	91.18
44	10.36	15.63	54.62	194.82	131.40	112.79
45	10.20	15.62	55.95	198.92	134.16	115.16
46	10.12	16.09	59.97	215.44	145.31	124.72
47	9.99	16.63	62.95	229.12	154.53	132.64
48	9.82	16.82	63.29	234.00	157.82	135.46
49	9.46	15.87	57.98	214.77	144.86	124.34

Conclusions

We study, along four profiles crossing Santiago de Cuba basin, the influence of the local soil conditions on seismic ground motion (*SH*-waves) due to earthquakes which occurred in the Oriente fault zone. A seismic zoning of the city has been done considering (1) the synthetic response spectra ratios (RSR) computed at sites along these profiles, (2) the surface geology and (3) the deeper structure of the basin. With the exception of four sites, where a big resonance effect, due to particular structural conditions, is present, all the RSR curves versus frequency have a common shape and differ only by their absolute value. Three different zones are identified. Each zone is characterized in terms of its expected ground motion parameters for two scenario earthquakes: the most probable ($M_S = 7$), and the maximum possible ($M_S = 8$). Where comparable, our results follow the general trend evidenced by previous investigations.

Acknowledgements

REFERENCES

ALVAREZ, L., ROMANELLI, F., and PANZA, G. F. (2001a), *Synthetic Seismograms in Laterally Heterogeneous Anelastic Media: Modal Summation for the Case of Offshore Seismic Sources* (*Deep-sea Trough*), The Abdus Salam ICTP Preprint IC/2001/169, 24 pp.

ALVAREZ, L., VACCARI, F., PANZA, G. F., and GONZÁLEZ, B. E. (2001b) *Modelling of Ground Motion in Santiago de Cuba City from Earthquakes in Oriente Fault Seismic Zone*, Pure Appl. Geophys. *158*, pp. 1763–1782.

ALVAREZ, L., VACCARI, F., and PANZA, G. F. (1999), *Deterministic Seismic Zoning of Eastern Cuba*, Pure Appl. Geophys. *156*, 469–486.

APPLIED TECHNOLOGY COUNCIL (1978), *Tentative Provisions for the Development of Seismic Regulations for Buildings*, U.S. National Bureau of Standards, Special Publication 510.

ARANGO, E. (1996), *Geodinámica de la región de Santiago de Cuba en el límite de las Placas de Norteamérica y el Caribe*, Tesis en opción al Grado de Master en Ciencias. Instituto Politécnico Nacional, México, D.F., 111 pp.

ARRIAZA, G. (1998), *Nuevos enfoques en la interpretación y procesamiento de las ondas refractadas para el estudio del basamento de Cuba*, Tesis presentada en opción al grado científico de Doctor en Ciencias Geológicas, La Habana, 179 pp.

AKI, K, *Strong motion seismology*. In *Strong Ground Motion Seismology*, NATO ASI Series, Series C: Mathematical and Physical Sciences, vol. 204 (eds. Erdik, M. Ö and Toksöz, M. N.) (D. Reidel Publishing Company, Dordrecht, 1987) pp. 3–41.

BERGE-THIERRY, C., LUSSOU, P., HERNÁNDEZ, B., COTTON, E., and GARIEL, J. C. (1999), *Computation of the strong motions during the 1995 Hyogoken-Nambu earthquake, combining the k-square spectral source model and the discrete wavenumber technique*. In *Proceedings of the Second International Symposium on the Effects of Surface Geology on Seismic Motion*, Yokohama, Japan, 1–3 December, 1998; Volume 3, The Effects of Surface Geology on Seismic Motion, Recent Progress and New Horizon on ESG Study, pp. 1414–1424.

BOVENKO, V. G., SHCHERBAKOVA, B. Ye., and HERNÁNDEZ, G. (1980), *New Geophysical Data on the Deep Structure of Eastern Cuba* (*in Russian*), Sov. Geol. *9*, 101–109.

COTILLA, M. and ALVAREZ, L. (1991), *Principios del mapa sismotectónico de Cuba*. Revista Geofísica del Instituto Panamericano de Geografía e Historia *35*, 113–124.

FÄH, D. (1992), *A Hybrid Technique for the Estimation of Strong Ground Motion in Sedimentary Basins*, Ph.D. Thesis, Nr. 9767, Swiss Fed. Inst. Technology, Zürich, 161 pp.

FÄH, D., IODICE, C., SUHADOLC, P., and PANZA, G. F. (1993), *A New Method for the Realistic Estimation of Seismic Ground Motion in Megacities, the Case of Rome*, Earthquake Spectra *9*, 643–668.

FÄH, D. and PANZA, G. F. (1994), *Realistic Modelling of Observed Seismic Motion in Complex Sedimentary Basins*, Ann. Geofis. *37*, 1771–1797.

FLORSCH, N., FÄH, D., SUHADOLC, P., and PANZA, G. F. (1991), *Complete Synthetic Seismograms for High-frequency Multimode SH-waves*, Pure Appl. Geophys. *136*, 529–560.

GONZÁLEZ, B. E. (1998), *El método de los microsismos en la solución de tarea de la sismología ingenieril*, Memorias del III Congreso cubano de Geología y Minería (GEOMIN98), Vol. I, pp. 284–286, Editorial Palcograf, ISSN 939-7117-01-0.

GUSEV, A. A. (1983), *Descriptive Statistical Model of Earthquake Source Radiation and its Application to an Estimation of Short-period Strong Motion*, Geophys. J. Roy. Astron. Soc. *74*, 787–800.

HARKRIDER, D. G. (1970), *Surface Waves in Multilayered Elastic Media. Part II. Higher Mode Spectra and Spectral Ratios from Point Sources in Plane Layered Earth Models*, Bull. Seismol. Soc. Am. *60*(6), 1937–1987.

ISHIHARA, K., Chairman (1993), *The Technical Committee for earthquake Geotechnical Engineering* (*TC-4*) *of the International Society for Soil Mechanics and Foundation Engineering, Manual for Zonation on Seismic Geotechnical Hazards*, The Japanese Society of Soil Mechanics and Foundation Engineering, 145 pp.

LEVANDER, A. R. (1988), *Fourth-order Finite-difference P-SV Seismograms*, Geophys. *53*, 1425–1436.

MEDINA, A., ESCOBAR, E., ORTÍZ, G. RAMÍREZ, M., DÍAZ, L., MÓNDELO, F., MONTEJO, N., DIÉGUEZ, H., GUEVARA, T., and ACOSTA, J. (1999), *Reconocimiento geólogo-geofísico de la cuenca de Santiago de Cuba, con fines de riesgo sísmico*, Empresa Geominera de Oriente, Santiago de Cuba, 32 pp., graphic annexes.

NORMA CUBANA (1999), *Propuesta de nueva norma cubana sismorresistente*, 110 pp. (draft).

ORIHUELA, N. and CUEVAS, J. L. (1993), *Modelaje sismogravimétrico de perfiles regionales del Caribe central*, Revista Ingeniería, Universidad Central de Venezuela *8*, 55–73.

PANZA, G. F. (1985), *Synthetic Seismograms: The Rayleigh Waves Modal Summation*, J. Geophys. Res. *58*, 125–145.

PANZA, G. F. and SUHADOLC, P. (1987), *Complete strong motion synthetics*. In (B. A. Bolt, ed.) *Seismic Strong Motion Synthetics*, *Computational Techniques* 4 (Academic Press, Orlando, 1987), pp. 153–204.

PANZA, G. F., VACCARI, F., COSTA, G., SUHADOLC, P., and FÄH, D. (1996), *Seismic Input Modelling for Zoning and Microzoning*, Earthquake Spectra, *12*, 529–566.

PANZA, G. F., ROMANELLI, F., and VACCARI, F. (2000), *Seismic Wave Propagation in Laterally Heterogeneous Anelastic Media: Theory and Applications to the Seismic Zonation*, *Advances in Geophysics*, Academic Press 43, 1–95.

PAVLOV, O. Y. (1984), *Seismic Microzoning* (in Russian), Moscow, Nauka.

PÉREZ, C. and GARCÍA, D., *Tectónica de la Sierra Maestra* (*Sureste de Cuba*). In *Estudios sobre Geología de Cuba* (eds Furrazola, G. and Núñez, K.) (Centro Nacional de Información Geológica, Instituto de Geología y Paleontología, La Habana, 1997) pp. 462–473.

PICO, R. (1999), *Determinación del umbral de semejanza β_0 para los algoritmos de agrupamiento lógico-combinatorios, mediante el dendrograma de un algoritmo jerárquico*. SIARP'99, IV Simposio Iberoamericano de Reconocimiento de Patrones. Memorias, pp. 259–265

RODRÍGUEZ, M., ALVAREZ, L., and GARCÍA, J. (1997), *Estimaciones probabilísticas de la peligrosidad sísmica en Cuba*, Revista Geofísica del Instituto Panamericano de Geografía e Historia, No. 47, pp. 46–77.

RUBIO, M. (1985), *The Assessment of Seismic Hazard for the Republic of Cuba*, Ph.D. Thesis, Institute of Geophysics, Science Academy of Czechoslovakia, Prague.

RUIZ, J., PICO, R., LÓPEZ, R., ALAMINOS, C., LAZO, M., BAGGIANO, M., BARRETO, E., SANTANA, A., ALVAREZ, L., and CHUY, T. (1992), *PROGNOSIS y sus aplicaciones a las geociencias*. In IBERAMIA-92, III Congreso Iberoamericano de Inteligencia Artificial, MEMORIAS. México, LIMUSA, pp. 561–586.

SEO, K., GONZÁLEZ, B. E., ARANGO, E., *et al.* (1998), *Past, Present and Perspective Research on Seismic Microzoning in the Cities of Santiago de Cuba and Havana*, Proceedings of the workshop to exchange research information in the international scientific research project "Joints Studies on Seismic Microzonation in Earthquake Countries," Tokyo Institute of Technology, Japan, 17 pp.

VAN DER HILST, R. D. (1990), T*omography with P, PP and pP Delay-time Data and the Three-dimensional Mantle Structure below the Caribbean Region*, Ph.D. Thesis, University of Utrecht.

VIRIEUX, J. (1984), *SH-wave Propagation in Heterogeneous Media: Velocity-stress Finite-difference Method*, Geophysics 49, 1933–1957.

VIRIEUX, J. (1986), *P-SV Wave Propagation in Heterogeneous Media: Velocity-stress Finite-difference Method*, Geophysics 51, 889–901.